© 2017. Published by The Company of Biologists Ltd | Development (2017) 144, 8-11 doi:10.1242/dev.146803

CORRESPONDENCE

Defective *adgra2* (*gpr124*) splicing and function in zebrafish *ouchless* mutants

Naguissa Bostaille[1], Anne Gauquier[1], Didier Y. R. Stainier[2], David W. Raible[3] and Benoit Vanhollebeke[1,4,*]

[1]Laboratory of Neurovascular Signaling, Department of Molecular Biology, ULB Neuroscience Institute, Université libre de Bruxelles (ULB), B-6041 Gosselies, Belgium.
[2]Department of Developmental Genetics, Max Planck Institute for Heart and Lung Research, 61231 Bad Nauheim, Germany.
[3]Department of Biological Structure, University of Washington, Seattle, WA 98195, USA.
[4]Center for Microscopy and Molecular Imaging, Université libre de Bruxelles (ULB), B-6041 Gosselies, Belgium.

*Author for correspondence (Benoit.Vanhollebeke@ulb.ac.be)

ABSTRACT

A hitherto unidentified N-ethyl-N-nitrosourea (ENU)-induced mutation affects dorsal root ganglia (DRG) formation in *ouchless* mutant zebrafish larvae. In contrast to previous findings assigning the *ouchless* phenotypes to downregulated *sorbs3* transcript levels, this work re-attributes the phenotypes to an essential splice site mutation affecting *adgra2* (*gpr124*) splicing and function. Accordingly, *ouchless* mutants fail to complement previously characterized *adgra2* mutants and exhibit highly penetrant cerebrovascular defects. The aberrantly spliced *adgra2* transcript found in *ouchless* mutants encodes a receptor lacking a single leucine-rich repeat (LRR) within its N-terminus.

KEY WORDS: *ouchless*, *sorbs3*, *adgra2*, *gpr124*, *reck*, Blood–brain barrier, Zebrafish

In a research article published in Development, Malmquist et al. (2013) phenotypically characterized the *ouchless* mutant that was recovered from an F3 forward genetic screen for defective dorsal root ganglion (DRG) neurogenesis. While the initial dorsoventral migration of neural crest-derived cell clusters towards presumptive DRG locales appears unaffected in *ouchless* mutants, the neurogenic program leading to the generation of *neurog1*:EGFP^{+} cells within the ganglion is defective, resulting in a severe reduction of DRG numbers in 72 hours post fertilization (hpf) *ouchless* mutants. *ouchless* mutants are viable but exhibit reduced growth rates and interrupted melanophore stripes in the adult skin. The *ouchless* mutation was mapped by bulk segregation analysis to a 342 kb genomic region of chromosome 8, harboring the *sorbs3* gene. No causative mutation could be identified within the coding sequence of *sorbs3*, but a mutation was suspected to reside within cis-regulatory elements, accounting for the reduced *sorbs3* transcript levels observed in *ouchless* mutants. Antisense *sorbs3* morpholino knockdown experiments, as well as BAC and mRNA rescue experiments, further supported the model that *sorbs3* regulates DRG neurogenesis and that *sorbs3* dysfunction drives the *ouchless* phenotypes (Malmquist et al., 2013).

The *ouchless* phenotypes are remarkably analogous to the DRG defects reported in *adgra2* (previously known as *gpr124*) mutants (Vanhollebeke et al., 2015). Adgra2 is a newly discovered Wnt7-specific co-activator of Wnt/β-catenin signaling (Posokhova et al., 2015; Vanhollebeke et al., 2015; Zhou and Nathans, 2014). Along with Reck, it has been shown to control DRG formation by activating Wnt signaling in neural crest-derived *sox10:*mRFP^{+} ganglion cells (Vanhollebeke et al., 2015). In addition, Adgra2 and Reck function as essential regulators of brain vascular development by promoting Wnt/β-catenin signaling in cerebrovascular endothelial cells (ECs) (Posokhova et al., 2015; Ulrich et al., 2016; Vanhollebeke et al., 2015; Zhou and Nathans, 2014). While the pivotal role of these proteins in cerebrovascular development is established both in the zebrafish and the mouse model (Anderson et al., 2011; Cullen et al., 2011; de Almeida et al., 2015; Kuhnert et al., 2010; Noda et al., 2016; Posokhova et al., 2015; Ulrich et al., 2016; Vanhollebeke et al., 2015; Zhou and Nathans, 2014), the molecular mechanisms underlying their activation and signal transduction remain to be determined. Given the phenotypic similarities, we therefore set out to test whether *adgra2* and *ouchless* (presumably *sorbs3*) co-operate during the process of DRG neurogenesis and brain vascularization.

We first tested whether *adgra2* and *ouchless* genetically interact by functional gene dosage experiments. Fish heterozygous for *ouchless* were crossed with the previously described *adgra2* heterozygotes, *adgra2*$^{s984/+}$ and *adgra2*$^{s985/+}$, and the offspring were assessed at 72 hpf for defects in DRG neurogenesis. From these crosses, ∼25% of the offspring (annotated as *ouchless/adgra2*^{s984} and *ouchless/adgra2*^{s985}) showed an almost complete lack of *neurog1*:EGFP^{+} DRG (Fig. 1A,A′). When raised to adulthood, these fish could be distinguished from their siblings by discontinuous dorsal melanophore stripes on their skin (Fig. 1A, brackets). As Adgra2 controls brain angiogenesis, we analyzed the cerebral vasculature of 60 hpf embryos derived from *ouchless* heterozygotes incrosses and outcrosses to *adgra2* heterozygotes. Strikingly, 25% of the offspring of each of the crosses displayed highly penetrant brain vascular defects, characterized by a complete absence of central arteries (CtAs), similar to *adgra2* mutants (Fig. 1B,B′). Further assessment using Wnt/β-catenin signaling reporter lines linked this phenotype to defective endothelial Wnt/β-catenin signaling in the perineural primordial hindbrain channel (PHBC) ECs (Fig. 1C). The lack of complementation between *ouchless* and *adgra2*, together with the discovery of vascular phenotypes in *ouchless* mutants that mimic those of *adgra2* mutants, raised the possibility that *ouchless* constitutes a new allele of *adgra2*. Accordingly, when *ouchless* mutants were injected at the one-cell stage with mRNA encoding wild-type (WT) Adgra2, significant restoration of *neurog1:*EGFP^{+} DRG (Fig. 1D,E) and cerebral blood vessels was observed (Fig. 1D,F).

We then re-evaluated the genomic region known to harbor the *ouchless* mutation and discovered that the *adgra2* gene resides within the critical interval, spanning the ca-48 and ca-37 genomic markers (Fig. 2A). This information was missing in the original characterization of the *ouchless* mutants owing to incomplete genome assembly and annotation at the time of analysis (Malmquist

Development (2017) 144, 8-11 doi:10.1242/dev.146803

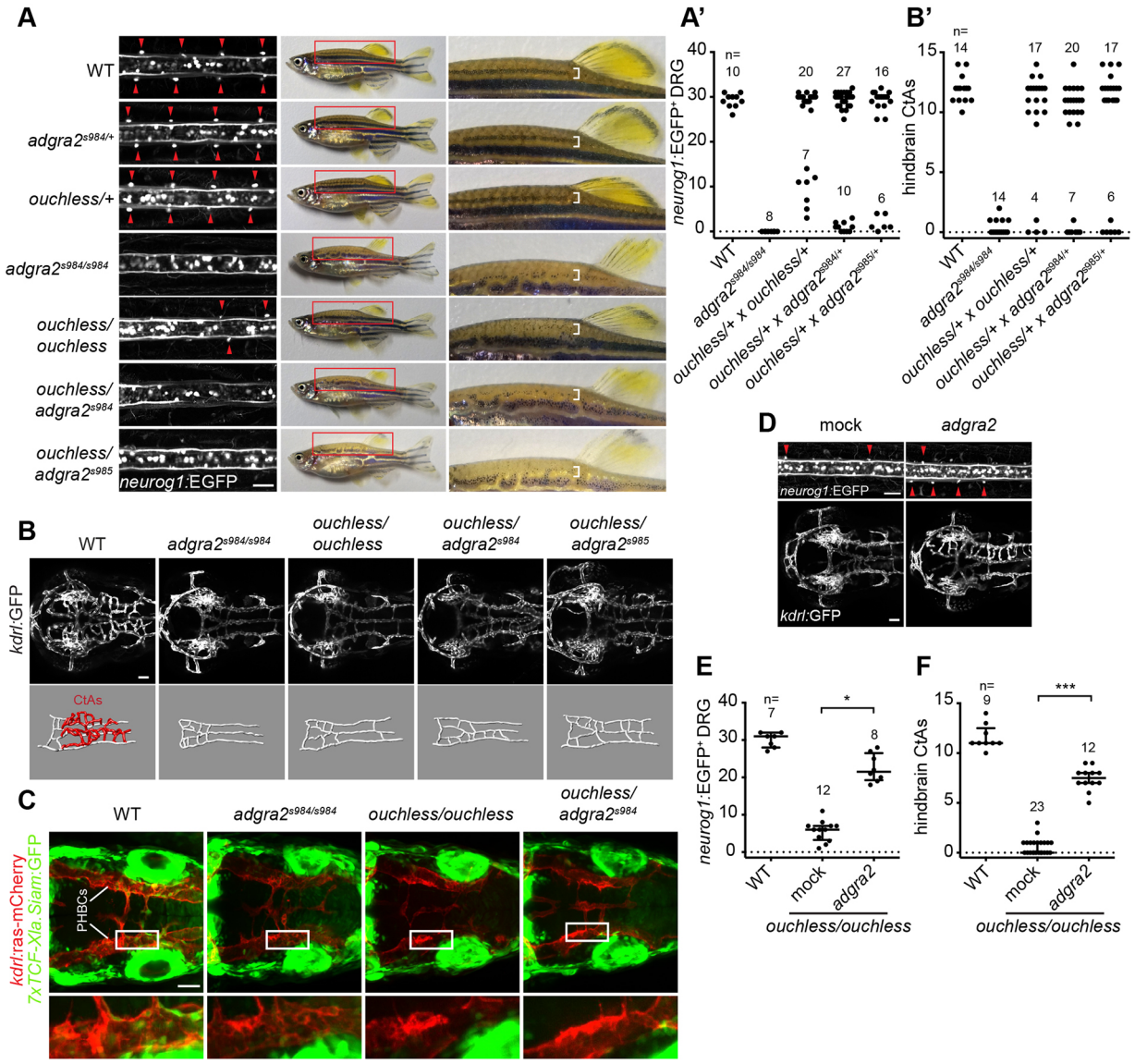

Fig. 1. *adgra2* and *ouchless* mutations fail to complement. (A) Dorsal views and (A′) quantification of EGFP$^+$ DRG neurons in 72 hpf *Tg(neurog1:EGFP)* larvae resulting from crossing *ouchless* and *adgra2* alleles. Red arrowheads indicate DRG neurons. Center and right columns illustrate the corresponding adult pigmentation patterns. The *neurog1*:EGFP$^+$ DRG were counted on one side of the 72 hpf larvae. Brackets indicate discontinuous dorsal melanophore stripes. (B) Confocal *z*-stack projections showing the brain vasculature of *Tg(kdrl:GFP)* WT and mutant embryos at 60 hpf in dorsal views (top) and 3D wire diagram representation of the cranial vessels, with intracerebral vessels (central arteries or CtAs) in red and perineural vessels in white (bottom). (B′) Quantification of the corresponding hindbrain CtAs. (C) Confocal projections in dorsal views of WT and mutant *Tg(7xTCF-Xia.Siam:GFP); Tg(kdrl:ras-mCherry)* embryos at 32 hpf. Boxes define the areas magnified in the bottom row. (D) Confocal projections of the *ouchless* mutant *Tg(neurog1:EGFP)* DRG at 72 hpf (top panels) and *Tg(kdrl:GFP)* cranial vasculature at 60 hpf (bottom panels) injected, or not, with 100 pg of *adgra2* mRNA at the one-cell stage. Red arrowheads indicate DRG neurons. (E) Quantification of *neurog1*:EGFP$^+$ DRG at 72 hpf and (F) hindbrain CtAs at 60 hpf in WT and *ouchless* mutant animals injected, or not, with 100 pg of *adgra2* mRNA at the one-cell stage. The *neurog1*:EGFP$^+$ DRG were counted on one side of the 72 hpf larvae. Error bars represent median ±interquartile range; **P*<0.05, ****P*<0.001 (Kruskal–Wallis test). PHBC, primordial hindbrain channel. Scale bars: 50 µm.

et al., 2013). We cloned the full-length *adgra2* coding sequence from *ouchless* mutants and evaluated the capacity of this allele to rescue DRG and CtA defects in *adgra2* morphants by mRNA injection at the one-cell stage. While mRNA encoding the WT receptor (annotated as *adgra2*) partially suppressed both phenotypes, the *ouchless* variant (annotated as *adgra2*^{ouchless}) did not affect either (Fig. 2D,E). Of note, the experiments were performed in morphants rather than mutants in order to increase the number of observations and hence the strength of the statistical analyses. The *adgra2* morpholino sequence and dosage used in this study were previously validated to ensure that phenotypic suppression values in morphant and mutant genetic backgrounds do not statistically differ (Vanhollebeke et al., 2015).

In order to identify the inactivating mutation, we compared a reference WT *adgra2* allele with the *adgra2* coding sequence recovered from *ouchless* mutant embryos. This analysis revealed four non-synonymous single nucleotide polymorphisms (SNPs; M429V, S895P, A1282V and A1302G) as well as an in-frame 72 bp deletion corresponding to exon 4 (Fig. 2C,F). While all four *adgra2* SNPs identified in *ouchless* mutants had been previously identified in functionally validated *adgra2* alleles derived from mixed AB/TL genetic backgrounds, alternative splicing resulting in exon 4

Development (2017) 144, 8-11 doi:10.1242/dev.146803

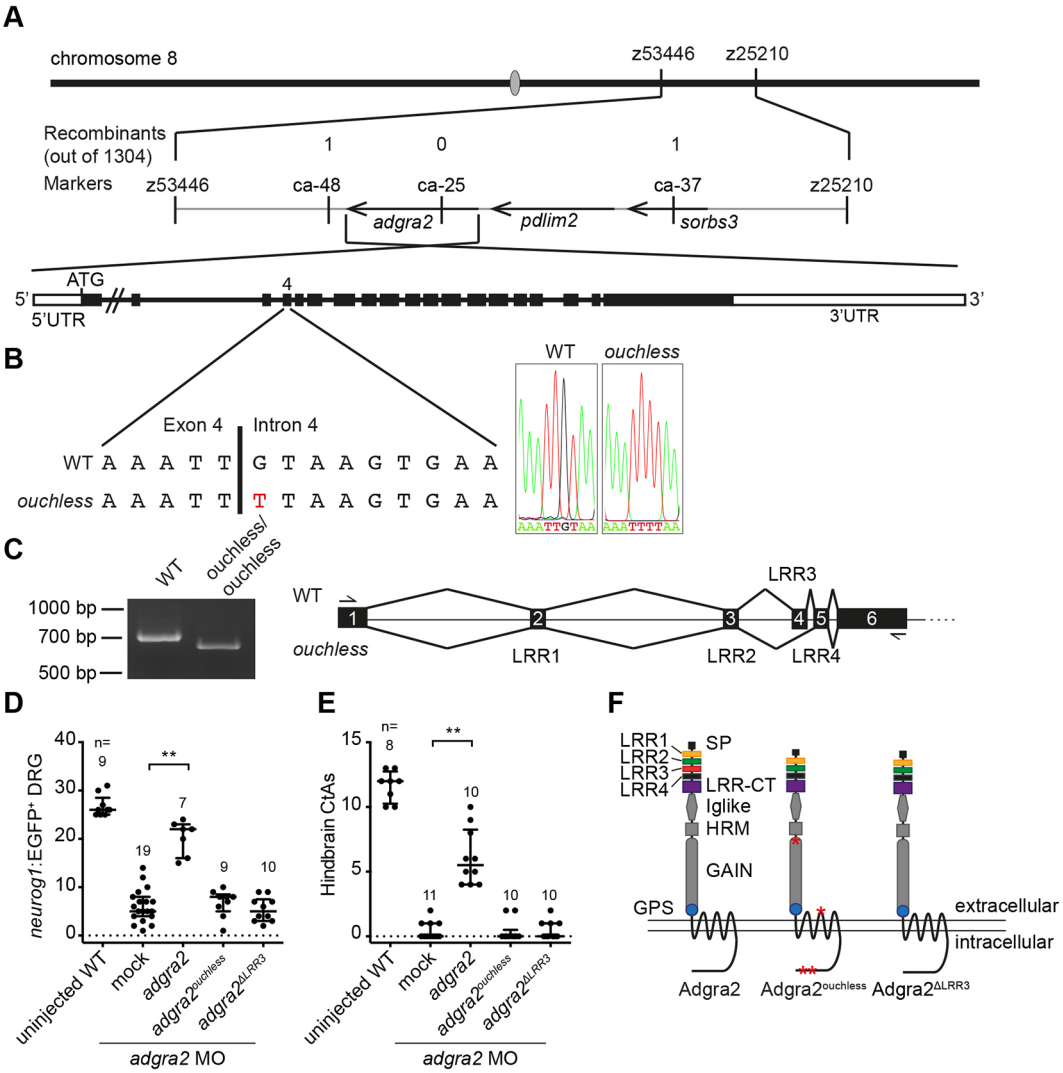

Fig. 2. *adgra2* is mutated in *ouchless* mutants. (A) Representation of the *ouchless* locus genetic map on chromosome 8. The number of recombinants among 1304 meioses as determined by Malmquist et al. (2013) is indicated above the markers utilized for mapping. (B) Sanger sequencing of the exon 4-intron 4 boundary of *adgra2* in WT and *ouchless* mutant embryos. The G→T change in the *ouchless* 5′ splice donor sequence appears in red. (C) RT-PCR splicing analysis of *adgra2* in 48 hpf WT and *ouchless* mutant embryos. The amplification primers hybridize to exon 1 and exon 6, as illustrated in the panel on the right. (D) Quantification of 72 hpf *neurog1*:EGFP^{+} DRG and (E) 60 hpf hindbrain CtAs in WT and *adgra2* morphants after injection of 100 pg of the indicated mRNA at the one-cell stage. Error bars represent median±interquartile range; $^{**}P<0.01$ (Kruskal–Wallis test). (F) Schematic representation of Adgra2, Adgra2^{ouchless} and Adgra2$^{\Delta LRR3}$ topology and domain organization. The red asterisks indicate the positions of the identified SNPs.

skipping is absent from any known zebrafish, mouse or human *ADGRA2* isoform. When probed in zebrafish, alternative splicing of the exon 1-exon 6 sequences is undetectable by RT-PCR (Fig. 2C) or by Sanger sequencing of full-length *adgra2* coding sequences derived from WT larvae (data not shown). Exon 4 corresponds precisely to the third leucine-rich repeat (LRR) unit of the LRR/CT domain of Adgra2, which comprises an array of four 24-residue-long LRR units followed by a LRR cysteine-rich C-terminal motif (LRR-CT) (Fig. 2F). Exon–protein domain correlations are recurrent amongst eukaryotes and reflect an efficient mechanism for protein modular functionalization through exon shuffling. The genomic structure of *ADGRA2* is evolutionary conserved, with LRR units precisely matching exons 2 to 5 in zebrafish, mouse and human (Fig. 2C). Sanger sequencing of genomic regions flanking *adgra2*^{ouchless} exon 4 identified an essential 5′ splice donor site mutation (GT→TT) at the exon 4–intron 4 boundary, which probably accounts for the exon 4 skipping event (Fig. 2B).

To confirm that the in-frame deletion of exon 4 leads to Adgra2 inactivation, we reproduced this deletion in a WT allele of *adgra2* by mutagenesis and evaluated the functionality of the resulting variant, *adgra2*$^{\Delta LRR3}$, in transient rescue assays. Injections of 100 pg of *adgra2*^{ouchless} or *adgra2*$^{\Delta LRR3}$ mRNA into *adgra2* morphants at the one-cell stage did not yield detectable rescuing neurogenic or angiogenic activity (Fig. 2D,E). This indicates that Adgra2 lacking LRR3 is functionally null. In light of this evidence, the fact that a limited number of DRG neurons develop in *ouchless* mutants, but not in the *adgra2*^{s984} and *adgra2*^{s985} frame-shift mutants, appears puzzling (Fig. 1A,A′). We speculate that the residual *ouchless* DRG neurons result either from a minor pool of normally spliced transcripts or from a cryptic splice-site activation event restoring a functional allele. However, these events must be very rare and tissue specific, as brain vascular defects of the *ouchless* and frame-shift mutants are equally penetrant and only the transcript lacking exon 4 could be amplified from 48 hpf *ouchless* mutants (Fig. 2C).

Development (2017) 144, 8-11 doi:10.1242/dev.146803

Altogether, this work reveals that *ouchless* and *adgra2* mutants are allelic and that the *ouchless* phenotypes result from an essential splice site mutation inactivating Adgra2 through the in-frame deletion of a single LRR in the ectodomain of this adhesion G-protein coupled receptor (GPCR). Further characterization of the *ouchless* allele suggests that the lack of this LRR motif impairs trafficking of Adgra2 (Bostaille et al., 2016).

Malmquist et al. (2013) previously attributed the *ouchless* phenotypes to defective *sorbs3* function based on convergent evidence from genomic mapping approaches, partial phenotypic rescue after ectopic Sorbs3 expression from cDNA or BAC templates as well as loss-of-function morpholino analyses. *sorbs3* was additionally reported to genetically interact with *erbb3* signaling in the process of DRG neurogenesis. We note that, while our current work unambiguously re-assigns the *ouchless* phenotypes to defective *adgra2* rather than *sorbs3*, it does not per se exclude (nor confirm) a role for *sorbs3* or *erbb3* in Adgra2-controlled DRG neurogenesis. However, in light of the genetic evidence presented here, a careful re-evaluation of their contribution to the *ouchless* phenotypes is warranted.

MATERIALS AND METHODS

Zebrafish strains and cell lines

Zebrafish (*Danio rerio*) were raised and maintained under standard conditions. The following lines were used: AB, TL, *Tg(kdrl:GFP)*^{s843} (Jin et al., 2005), *Tg(kdrl:ras-mCherry)*^{s896} (Chi et al., 2008), *Tg(7xTCF-Xla.Siam:GFP)*^{ia4} (Moro et al., 2012), *Tg(-17.0neurog1:EGFP)*^{w61} (McGraw et al., 2008), *ouchless* (*sorbs3*^{w35}) (Malmquist et al., 2013), *adgra2*^{s984} and *adgra2*^{s985} (Vanhollebeke et al., 2015), as reported previously. All animal experiments were performed in accordance with the rules of the State of Belgium (protocol approval number: CEBEA-IBMM-2012:65).

Cloning strategy, morpholino and RNA expression constructs

The *adgra2*$^{\Delta LRR3}$ deletion mutant was generated by In-Fusion cloning (Takara, Mountain View, CA) and the deletion corresponds to amino acids 125-148. Capped messenger RNA was synthesized using the mMESSAGE mMACHINE kit (Ambion, Carlsbad, CA). In all panels, one-cell-stage embryos were injected either with 100 pg of the indicated mRNA or 4 ng of a previously validated *adgra2* splice-blocking morpholino (Vanhollebeke et al., 2015).

Imaging

Images were acquired on a Zeiss LSM710 confocal microscope. Three-dimensional representations were generated using Imaris FilamentTracer software (BitPlane, Zurich, Switzerland).

Statistical analysis

Statistical analyses were performed using the GraphPad Prism software. Sample size was determined with G*power v.3.1.5 software to reach adequate statistical power. Each dot plot value represents an independent embryo and every experiment was conducted three times independently. *P*-values were calculated by the Kruskal–Wallis test (*post hoc* Dunn's test).

Acknowledgements

We thank the B.V. laboratory members for critical reading of the manuscript and E. Dupont for technical assistance.

Competing interests

The authors declare no competing or financial interests.

Funding

N.B. is supported by a FRIA fellowship from Fonds de la Recherche Scientifique - FNRS. Work in the B.V. laboratory is supported by the FNRS (MIS F.4543.15), a Concerted Research Action (ARC) grant from the Fédération Wallonie-Bruxelles and the Fondation Université libre de Bruxelles. The Center for Microscopy and Molecular Imaging (CMMI) is supported by the European Regional Development Fund (ERDF).

References

Anderson, K. D., Pan, L., Yang, X., Hughes, V. C., Walls, J. R., Dominguez, M. G., Simmons, M. V., Burfeind, P., Xue, Y., Wei, Y. et al. (2011). Angiogenic sprouting into neural tissue requires Gpr124, an orphan G protein-coupled receptor. *Proc. Natl. Acad. Sci. USA* **108**, 2807-2812.

Bostaille, N., Gauquier, A., Twyffels, L. and Vanhollebeke, B. (2016). Molecular insights into Adgra2/Gpr124 and Reck intracellular trafficking. *Biol. Open* **5**, 1874-1881.

Chi, N. C., Shaw, R. M., De Val, S., Kang, G., Jan, L. Y., Black, B. L. and Stainier, D. Y. R. (2008). Foxn4 directly regulates tbx2b expression and atrioventricular canal formation. *Genes Dev.* **22**, 734-739.

Cullen, M., Elzarrad, M. K., Seaman, S., Zudaire, E., Stevens, J., Yang, M. Y., Li, X., Chaudhary, A., Xu, L., Hilton, M. B. et al. (2011). GPR124, an orphan G protein-coupled receptor, is required for CNS-specific vascularization and establishment of the blood-brain barrier. *Proc. Natl. Acad. Sci. USA* **108**, 5759-5764.

de Almeida, G. M., Yamamoto, M., Morioka, Y., Ogawa, S., Matsuzaki, T. and Noda, M. (2015). Critical roles for murine Reck in the regulation of vascular patterning and stabilization. *Sci. Rep.* **5**, 17860.

Jin, S.-W., Beis, D., Mitchell, T., Chen, J.-N. and Stainier, D. Y. R. (2005). Cellular and molecular analyses of vascular tube and lumen formation in zebrafish. *Development* **132**, 5199-5209.

Kuhnert, F., Mancuso, M. R., Shamloo, A., Wang, H.-T., Choksi, V., Florek, M., Su, H., Fruttiger, M., Young, W. L., Heilshorn, S. C. et al. (2010). Essential regulation of CNS angiogenesis by the orphan G protein-coupled receptor GPR124. *Science* **330**, 985-989.

Malmquist, S. J., Abramsson, A., McGraw, H. F., Linbo, T. H. and Raible, D. W. (2013). Modulation of dorsal root ganglion development by ErbB signaling and the scaffold protein Sorbs3. *Development* **140**, 3986-3996.

McGraw, H. F., Nechiporuk, A. and Raible, D. W. (2008). Zebrafish dorsal root ganglia neural precursor cells adopt a glial fate in the absence of neurogenin1. *J. Neurosci.* **28**, 12558-12569.

Moro, E., Ozhan-Kizil, G., Mongera, A., Beis, D., Wierzbicki, C., Young, R. M., Bournele, D., Domenichini, A., Valdivia, L. E., Lum, L. et al. (2012). In vivo Wnt signaling tracing through a transgenic biosensor fish reveals novel activity domains. *Dev. Biol.* **366**, 327-340.

Noda, M., Vallon, M. and Kuo, C. J. (2016). The Wnt7's Tale: a story of an orphan who finds her tie to a famous family. *Cancer Sci.* **107**, 576-582.

Posokhova, E., Shukla, A., Seaman, S., Volate, S., Hilton, M. B., Wu, B., Morris, H., Swing, D. A., Zhou, M., Zudaire, E. et al. (2015). GPR124 functions as a WNT7-specific coactivator of canonical β-catenin signaling. *Cell Rep.* **10**, 123-130.

Ulrich, F., Carretero-Ortega, J., Menendez, J., Narvaez, C., Sun, B., Lancaster, E., Pershad, V., Trzaska, S., Veliz, E., Kamei, M. et al. (2016). Reck enables cerebrovascular development by promoting canonical Wnt signaling. *Development* **143**, 147-159.

Vanhollebeke, B., Stone, O. A., Bostaille, N., Cho, C., Zhou, Y., Maquet, E., Gauquier, A., Cabochette, P., Fukuhara, S., Mochizuki, N. et al. (2015). Tip cell-specific requirement for an atypical Gpr124- and Reck-dependent Wnt/β-catenin pathway during brain angiogenesis. *eLife* **4**, e06489.

Zhou, Y. and Nathans, J. (2014). Gpr124 controls CNS angiogenesis and blood-brain barrier integrity by promoting ligand-specific canonical Wnt signaling. *Dev. Cell* **31**, 248-256.

10.1242/dev.146803